ARTICLE

Check for updates

Anomalous elasticity and damping in covalently cross-linked graphene aerogels

Martin Šilhavík[1,2], Prabhat Kumar[1], Zahid Ali Zafar[1,3], Martin Míšek[4], Martin Čičala[2,5], Marek Piliarik [5] &
Jiří Červenka [1✉]

Elasticity in materials is a phenomenon that provides a basis for widespread practical applications in engineering, medicine, and electronics. Most of the conventional materials can withstand only small deformations within the elastic limit, typically below 5% of their original size. Here, we report a graphene aerogel made of covalently cross-linked graphene sheets that exhibits anomalous superelastic behavior up to 92% of compressive and 68% tensile strain. We show that the graphene aerogel has a nonlinear stress-strain characteristic with the compressive and tensile yield strength of 4.5 GPa and 0.6 MPa, respectively. By considering the elastic bending of graphene sheets and buckle folding of pore walls, we develop a quantitative origami model that describes the stress-strain behavior of the aerogel. In addition, we analyze the mechanical oscillations of the graphene aerogel, observing superfast vibration damping within a time scale of 50–250 ns. Our study demonstrates the unusual coexistence of superelasticity and superfast damping within a cellular material with atomically thin pore walls, a phenomenon that does not occur in bulk elastic materials described by Hook's law.

[1] Department of Thin Films and Nanostructures, Institute of Physics of the Czech Academy of Sciences, Cukrovarnická 10/112, 162 00 Prague, Czech Republic. [2] Department of Physical Electronics, Faculty of Nuclear Sciences and Physical Engineering, Czech Technical University, Trojanova 13, 120 00 Prague, Czech Republic. [3] Department of Physical Chemistry and Macromolecular Chemistry, Faculty of Science, Charles University in Prague, Hlavova 2030, 128 43 Prague, Czech Republic. [4] Department of Magnetics and Superconductors, Institute of Physics of the Czech Academy of Sciences, Cukrovarnická 10/112, 162 00 Prague, Czech Republic. [5] Institute of Photonics and Electronics of the Czech Academy of Sciences, Chaberská 1014/57, 182 51 Prague, Czech Republic. ✉email: cervenka@fzu.cz

E lasticity is the ability of a deformed material to return to its original shape and size when the forces causing the deformation are removed. Materials capable of withstanding large elastic strains and resisting permanent deformation during load have a profound effect on day-to-day lives. They are used in a plethora of applications, in the construction, automotive, biomedicine, electronics, and aerospace industries. These materials enable the fabrication of tension/pressure-bearing components, flexible electronic devices, sensors, advanced spring, contact fatigue, and wear-resistant applications. In the continual quest for better materials, researchers have been searching for stronger elastic materials that can withstand larger mechanical loads with minimal plastic deformation[1,2]. However, larger values of the elastic modulus usually tend to lower the extensibility and compressibility of a material[3]. To increase the resilience of materials, different strategies for controlling the construction of elastic materials on the atomic level and microstructure have been intensively studied[4–7]. Recent developments have shown that a clever architectural design in the construction of porous and cellular materials can offer intriguing mechanical properties and superelasticity[1,8], providing an effective way to extend the elastic strain range in compression beyond the small deformation limit. However, the porous materials reported so far have suffered from substantial degradation in tensile strength and modulus[9]. Highly stretchable elastic materials based on polymeric and silicone rubbers, on the other hand, demonstrate small yield strength in compression[10]. Materials of high strength that would sustain both large elastic deformation in compression and tension have not been developed yet, despite such a mechanical behavior is displayed by biological materials[3]. This requires a smart material design that integrates high porosity, high-strength, large-strain elasticity, and variable density in a single material.

In recent years, 3D porous graphene aerogels and foams have attracted significant attention because they demonstrate a rich variety of physical properties, including superelasticity in compression[11], good electrical conductivity[12], and piezoresistivity under a mechanical strain[13]. These properties have been utilized in the development of electromechanical sensors, which have demonstrated exceptionally large elastic strain, sensitivity, and fast response in compression[14–16]. However, the ultimate elastic limit of graphene aerogels in compression has not been

determined yet[17]. Moreover, the 3D porous graphene materials still suffer from a significant hysteresis and limited elasticity range in tensile[18,19]. The highest tensile strain reported in 3D porous graphene grown by chemical vapor deposition has been 17.5% at a stress of 255 kPa[19]. The low tensile elasticity and strength of 3D graphene materials are mainly caused by a weak coupling of individual graphene sheets[20] and a high number of defects[21] in these materials.

Here, we demonstrate that the covalent cross-linking of graphene sheets in a 3D porous graphene aerogel enables achieving both large compressive and tensile elasticity without significantly degrading the specific strength of the material. The covalently cross-linked graphene aerogels manifest the largest superelastic range and specific compressive yield strength observed in a material so far. We show that the anomalous superelastic behavior of the 3D graphene aerogel is governed by the high bending flexibility of graphene, which allows multiple buckle folding of pore walls in the aerogel in a similar fashion to origami. As a result, the graphene aerogel exhibits variable stiffness, density, and electrical conductivity when gradually deformed. More surprisingly, we find that the materials display unusual vibration damping properties, which enable superfast damping and response to nanosecond mechanical processes. These observations highlight the unique and rich electromechanical behavior of 3D graphene materials arranged in a cellular structure.

Result and discussion

Synthesis. The graphene aerogel is fabricated using a hydrothermal synthesis from a graphene oxide powder followed by freeze-drying (Fig. 1a)[22]. The as-prepared aerogel has a 3D porous structure with micrometer-sized pores composed of few-layer graphene (Fig. 1b). The chemical analysis using X-ray photoelectron spectroscopy (XPS) shows that the graphene oxide is only partly reduced after the hydrothermal synthesis (Fig. 1c). The chemically reduced graphene oxide aerogel contains 82% of carbon and 18% of oxygen. To remove the remaining oxygen from the aerogels, we used high-temperature annealing at 1300 °C in a vacuum for 30 min. Such a high annealing temperature has been selected because it exceeds the desorption temperature of all known oxygen species in graphene, which have been reported to
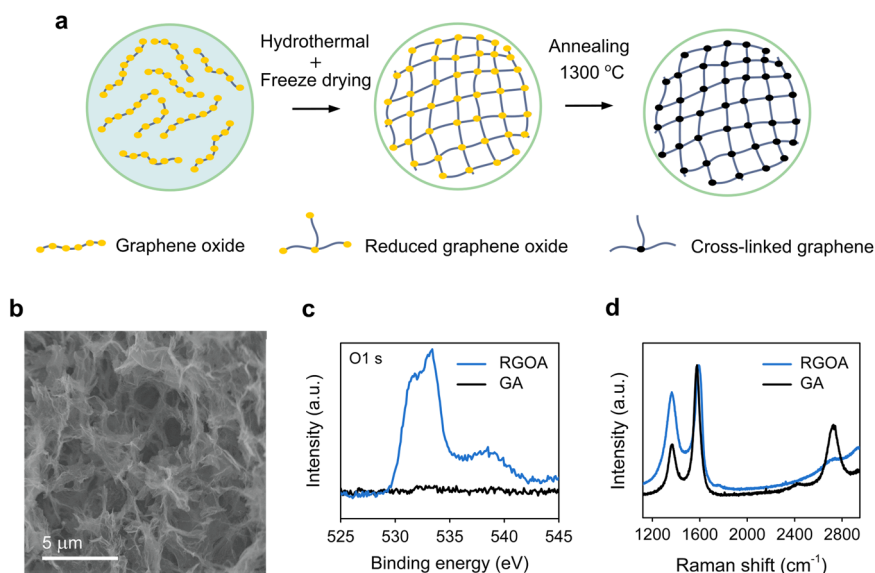

Fig. 1 Structure and chemical composition of graphene aerogels. a Schematics of the fabrication process of the cross-linked graphene aerogel. **b** Scanning electron micrograph of the porous structure of graphene aerogel. **c** X-ray photoelectron spectroscopy O 1s spectra of a reduced graphene oxide aerogel (RGOA) and the annealed graphene aerogel (GA). **d** Raman spectra of the graphene aerogels before and after the annealing.
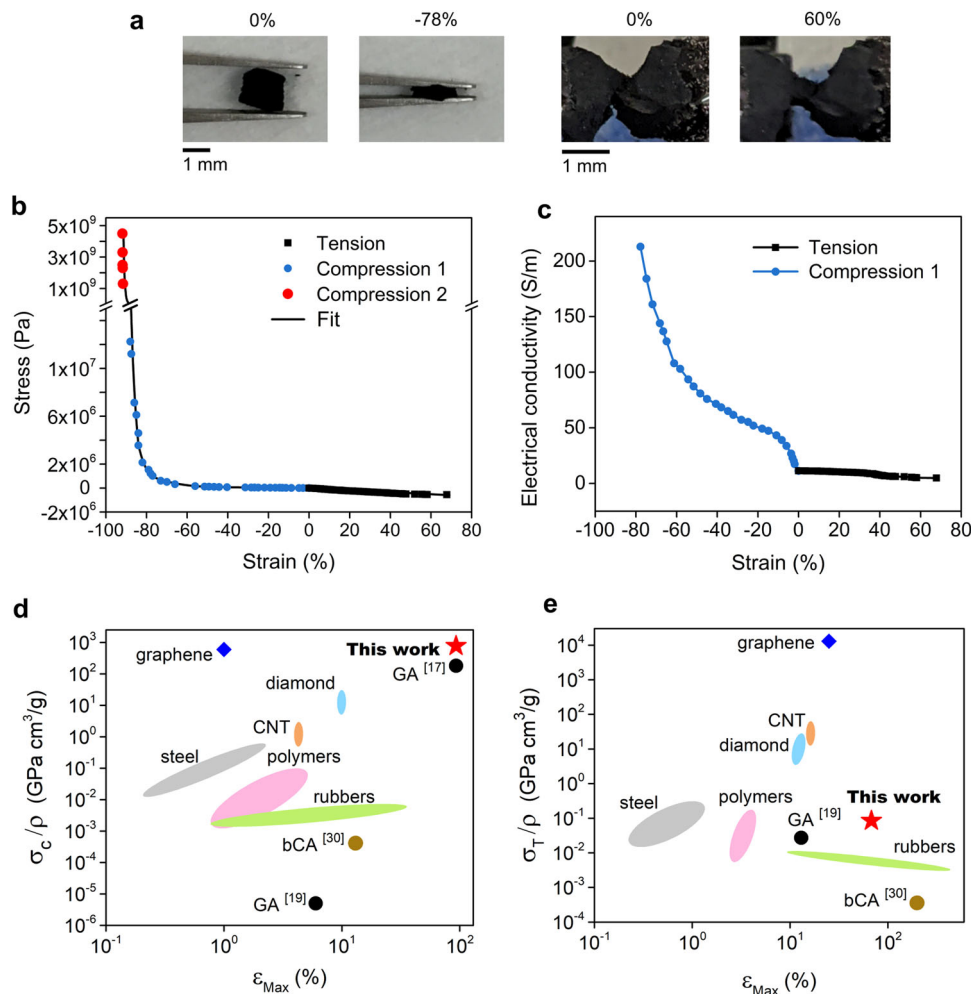
Fig. 2 Mechanical and electrical properties of graphene aerogels. a Optical image of macroscopic samples under compressive (−78%) and tensile (60%) strain. The positive and negative strain is used to distinguish between tensile and compressive deformation, respectively. **b** Compressive and tensile stress-strain curves of graphene aerogel. The negative stress depicts the opposite direction to the applied pressure. Each point represents an average of $N = 10$ experiments. Error bars are smaller than the symbol size, see Methods Mechanical testing for full statistics. **c** Electrical conductivity as a function of compressive (negative) and tensile (positive) strain. **d**, **e** Comparison of compressive[44-49] (**d**) and tensile[50-55] (**e**) specific yield strength of different materials (graphene aerogels (GA)[17,19], binary carbon aerogels (bCA)[29], graphene[45,51], diamond[46,52], CNT[47,53], stainless steel[48,54], polymers[49,55], and elastomers[36,50]) as a function of the maximum elastic strain.

desorb at temperatures of 1100 °C or below[23–26]. The high-temperature annealing has deoxidized the graphene aerogel and improved its crystallinity, as confirmed by XPS and Raman spectroscopy (Fig. 1c, d and Supplementary Table 1). The level of oxygen in the annealed aerogels is below the resolution limit of the XPS technique (<0.6%). The porous structure of the aerogel has not been affected by the annealing as observed by scanning electron microscopy (SEM) (Supplementary Fig. 1). More interestingly, the high-temperature annealing has led to the covalent cross-linking of the graphene sheets in the aerogel. We anticipate that the broken C–O bonds have been transferred to C–C bonds at the overlap of two graphene sheets in a pyrolytic process similar to the pyrolysis of carbon fiber reinforced polymers[27,28]. The formation of the C–C covalent cross-linking in the graphene aerogels is confirmed below by a significant improvement of the mechanical strength[27] and an increase of the electrical conductivity[12] after the annealing.

Mechanical properties. Figure 2 shows the mechanical and electrical properties of the cross-linked graphene aerogels as a function of compressive and tensile strain. The positive and negative strain is used to distinguish between elongation and compression, respectively. The negative values of stress indicate tension (the opposite direction to the pressure). The static compression testing was done on a millimeter-sized sample using a mechanical press (low pressures - Supplementary Fig. 2) and a diamond anvil cell (high pressures - Supplementary Fig. 2). The strain was determined using an optical microscope (Supplementary Method 2). The elasticity at high pressures was determined from the reversibility of the Raman G band (Supplementary Fig. 3 and Supplementary Table 3). The tensile test was performed on a graphene aerogel specimen with reduced volume in the center and two edge-glued joints (Supplementary Figs. 4–6 and Supplementary Movies 1, 2). The stress-strain curve of the graphene aerogel subjected to the compression-tension test (Fig. 2b) shows a complex nonlinear behavior with a steep rise at high pressures (< −60% strain). The electrical conductivity of the sample exhibits a similar trend to the stress-strain characteristics. The conductivity changes by two orders of magnitude over the whole measured strain range, enabling detection of the mechanical strain of all biological materials[3,29]. The mechanical behavior of the graphene aerogel is highly reversible, demonstrating superelasticity over a wide deformation range of −92% compressive and 68% tensile

strain. After removing the load, the aerogel exhibits an instant and complete recovery of the sample size and shape. The reversibility has been observed even after 5000 compressive loading cycles (Supplementary Method 4, Supplementary Fig. 7 and Supplementary Movies 3, 4). The maximum elastic yield strength of the graphene aerogel is 4.5 GPa in compression and 0.6 MPa in tensile. The comparison of compressive and tensile yield strength of our material to different graphene-based aerogels is in Supplementary Note 1. If we relate the measured compressive yield strength relative to the density of the graphene aerogel, we get the specific strength of $770\,\text{GPa}\,\text{cm}^3\,\text{g}^{-1}$. This specific strength is several orders of magnitude larger than the specific compressive strength of the conventional construction materials and other carbon allotropes (Fig. 2d and Supplementary Table 2). The observed strength and elastic range also exceed the previous records reported for highly compressible graphene aerogels (GA)[17,19] and binary carbon aerogels (bCA)[29]. The range of elasticity and specific strength of our graphene aerogel in tensile are also significantly larger than in previous porous graphene materials (Fig. 2e and Supplementary Table 2)[17,30]. In tensile, the specific strength of the graphene aerogel is $0.1\,\text{GPa}\,\text{cm}^3\,\text{g}^{-1}$ (Fig. 2e), which is similar to the specific strength of stainless steel but at an order of magnitude larger elastic strain. This is because the graphene aerogel has a significantly larger modulus of resilience, which is $2.3 \times 10^7\,\text{J}\,\text{m}^{-3}$ in tensile and $3.2 \times 10^9\,\text{J}\,\text{m}^{-3}$ in compression.

The observed high tensile strength of the graphene aerogel provides direct evidence of our hypothesis of the covalent cross-linking of graphene sheets in the material[30,31]. Non-covalently bonded aerogel would not withstand such high forces, mainly due to the extremely low sliding resistance of graphene flakes stacked one on top of each other[32], which should result in permanent deformation of the aerogels at relatively small loads. The same argument can be used for the high-pressure experiments, where it is very unlikely that a weakly bonded graphene aerogel would return to its original size and shape after compressing it to 4.5 GPa. By assuming the typical rupture force (F_i) of a single covalent C–C (or C=C) bond of the length of 1.54 nm (1.33 nm) under stretching 4.1 nN (7.3 nN)[33] and the tensile strength (σ_T) of the graphene aerogel with a surface area of $0.45\,\text{mm}^2$ (S), we estimate that the amount of carbon cross-linking $n_{C-C} = \frac{\sigma_T \times S}{F_i}$ in the aerogels is $\sim 1.5 \times 10^8$ per mm^2 ($n_{C=C} = 3.7 \times 10^7$ per mm^2). This estimate suggests that the amount of the C–C cross-linking in the material is still relatively small (<0.3%) and can be significantly improved. In the ideal situation, the specific tensile strength of a completely cross-linked 3D graphene aerogel might approach the tensile strength of 2D graphene ($573\,\text{GPa}\,\text{cm}^3\,\text{g}^{-1}$)[34]. It is also expected that a higher amount of covalent cross-linking in the aerogels could diminish the occurrence of defects in the porous structure[35]. Local defects and cracks in the graphene aerogels have been found susceptible to local stress concentration and crack extension in the tensile testing, resulting in significant degradation of the tensile strength of the materials (Supplementary Table 4 and Supplementary Fig. 6).

Analytical model of compression. To understand the unusual mechanical behavior, we investigated the deformation of individual pores in the graphene aerogels under compression using in situ scanning electron microscopy (Fig. 3a). It was observed that the pores get gradually deformed until a point (~50% strain) when they undergo a collapse into two pores (Supplementary Fig. 8). Based on this observation we propose a modular origami bending/folding model that can fit the measured stress-strain curves (Fig. 2b and Supplementary Discussion 1) and the density-strain change of the graphene aerogels under compression

(Fig. 3b). Our model is fundamentally different from the density scaling model of open cellular materials reported before[19], which predicts power scaling of the elastic modulus and yield strength with specific density. The density scaling model cannot be applied in our system because it is based on linear stress-strain behavior. The observed steep nonlinear stress-strain characteristics of the covalently cross-linked graphene aerogels cannot also be explained by any previous graphene network models[2].

Our modular origami model is based on an array of interconnected spherical springs (Supplementary Fig. 8), which elastically bend and undergo multiple buckle folds as the pressure is increasing (Fig. 3c). We assume that the spring corresponds to an average pore in the aerogel with a mean diameter of 1 μm and a thin wall consisting of few-layer graphene. The sphere buckles elastically under the applied pressure (Fig. 3b) at the critical pressure (p_c) of buckling[36]

$$p_C = \frac{2nE}{\sqrt{3(1-\gamma^2)}}\left(\frac{h}{R}\right)^2,$$

where E is the Young modulus of few-layer graphene (0.5 TPa)[37], n is a relative Young modulus constant which is used as a first fitting parameter, h is the thickness of the pore (1.5 nm), R is the average pore's radius (1 μm as determined from SEM), and γ is the Poisson's ratio (0.03 as determined from optical measurements). The model assumes that the sum of the surface area of the graphene walls of the original pore remains unchanged after all consequential pore collapses. Hence, the radius of the original pore (R) needs to satisfy $R^2 = (R_1 m)^2 = (R_2 m^2)^2 = \ldots = (R_H m^H)^2$, where m is a second fitting parameter determining the number of the created pores after the buckling, and R_H is the minimum elastic bending radius of graphene. The stress (σ) and strain (ε) model of graphene aerogel can be expressed as (Supporting Information)

$$\sigma = \sigma_{\text{lin}} + \sigma_{\text{non-lin}} = \frac{l}{A}(k_{\text{lin}} + k_{\text{non-lin}})\varepsilon,$$

where the stress-strain behavior is following a linear relationship (σ_{lin}) according to Hooke's law in the first linear region until the first critical pressure of pore buckling is reached, and a nonlinear relationship ($\sigma_{\text{non-lin}}$) in the second region due to the multiple buckle folding of pores. In the linear region, k_{lin} denotes the total spring constant of all interconnected pores, l is the length of the sample, and A is the area of the sample under the pressure. Once the buckling takes place the total spring constant changes to $k_{\text{non-lin}}$ due to an increasing density of the aerogel caused by the division of pores into a larger number of smaller buckled pores. The nonlinear spring constant is a sum of multiple linear spring constants that are representing the elasticity of the buckled pores in between two critical pressures of the buckle folding, p_{c1}, p_{c2}, ..., $p_{c(H-1)}$ (Supplementary Discussion 1). As the buckling continues, the density of pores increases in the aerogel as the pores elastically fold into a smaller and smaller volume until reaching the minimum elastic bending radius at the critical pressure. The fit of the experimental data (Supplementary Fig. 9 and Supplementary Table 5) using the origami model estimates that m is close to 2 and there are seven buckling collapses in the fully compressed graphene aerogel with the minimum elastic bending radius of 12 nm at 4.5 GPa. This bending radius is still far from the theoretical minimum elastic bending radius of monolayer graphene (1 nm)[38], which should result in nine buckling collapses. The model determines that the critical buckling limit of the first collapse is at 53% strain, which is in line with the experimental observations.

The energy dissipated in the aerogel during one cycle of loading and unloading up to the first pore buckling collapse is very small (~3%), as demonstrated by a negligible hysteresis of
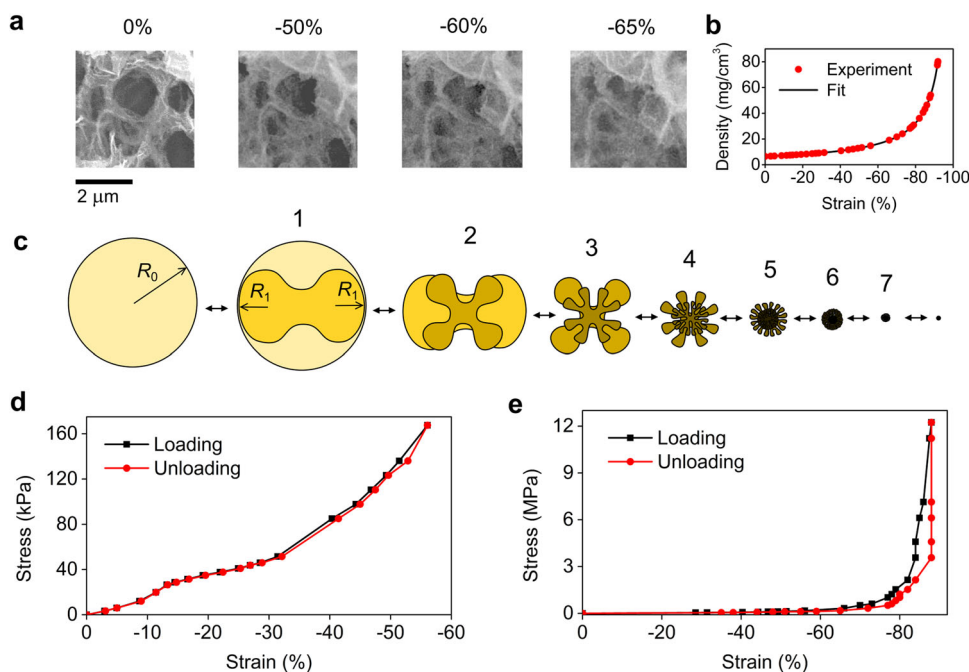
Fig. 3 Buckling of pores in graphene aerogels. a In situ scanning electron microscopy images of graphene aerogel under compression at 0, −50, −60, and 65% strain. **b** Density of the graphene aerogel as a function of strain. **c** Schematic visualization of multiple pore collapses in the origami model. **d, e** Loading and unloading stress-strain curves of a graphene aerogel up to 56% (**d**) and 88% strain (**e**). Error bars are smaller than the symbol size, see Methods Mechanical testing for full statistics.

the stress-strain curves (Fig. 3d). However, the two paths of stress-strain curves diverge above the critical buckling limit (>53% strain) (Fig. 3e). The energy loss after two buckling collapses determined from the area between the stress-strain curves at 88% strain is 42%. This result suggests that the sudden sideways buckling of few-layer graphene requires additional energy. However, this energy is stored chiefly in the system in the form of strain energy, as demonstrated by a rapid response of the aerogel upon the dynamic loading. It is important to mention that the observed hysteresis in our stress-strain curves is significantly smaller than in previous reports on graphene aerogels[17,30], which is attributed to the smaller oxygen content in our materials.

Damping. The dynamic deformation of graphene aerogel blocks was studied using a bouncing ball stimulation by a high-speed camera (Fig. 4a and Supplementary Movie 5). The graphene aerogel reacted immediately at the measured framerate and followed the path of the bouncing ball back to the original position without any vibration after the impact. A similar observation of the fast (millisecond) reaction of a graphene aerogel to a bouncing ball has been reported before[1]. However, the observed dynamic response of graphene aerogel is different from the dynamic response of common elastic stainless steel springs and polymeric foams (Fig. 4a and Supplementary Movies 6, 7). A steel spring also responded elastically to the bouncing ball but the impact was followed by spring oscillations. A polymeric foam demonstrated a typically plastic response, showing an incomplete recovery after the impact and long-term shrinkage. As the fast camera was not able to measure any vibration of the graphene aerogel even at high deformation (>50% strain) in the millisecond time range, we measured the vibrations of the sample from the voltage change at a constant electrical current using an oscilloscope down to a nanosecond regime. The electrical detection of the sample deformations was possible because the electrical conductivity of the graphene aerogel is highly sensitive to mechanical strain (Fig. 2c). The electrically determined

mechanical vibrations of mechanically excited graphene aerogel samples have shown underdamped oscillations with a resonance frequency (f_R) and damping ratio (ζ) of the range of 20–150 MHz and $0.2–2.3 \times 10^7$, respectively (Fig. 4b–f and Supplementary Table 6). The mechanical oscillations induced by a metal rod impact were damped in a millimeter-sized graphene aerogel sample below the amplitude of 1 μm within 50–250 ns (Fig. 4b and Supplementary Fig. 10). Such a fast damping process has not been observed in any macroscopic elastic material before. For instance, micrometer-sized mechanical resonators based on a freestanding few-layer graphene membrane have demonstrated a significantly slower damping time of ~20 μs[39].

To get insight into the origin of the nanosecond mechanical damping in graphene aerogels, we examine how the resonant frequency and damping ratio change as a function of the sample size and external pressure (Fig. 4c–f). Results show that the resonant frequency of the sample increases with decreasing pressure. This is in line with the expected decrease of the drag force exerted by the gasses on the moving sample in a vacuum. However, the oscillations of the graphene aerogel are damped faster at lower pressures, resulting in a higher damping ratio in a vacuum. The graphene aerogel has also shown no noticeable change of the resonant frequency and damping ratio when we reduced the cross-section area (ΔA) of the aerogel block while keeping the same thickness. The observed behavior is completely different from the behavior of the standard Hookean underdamped harmonic oscillator. The resonant frequency and damping ratio in the Hookean oscillator should vary significantly with the cross-section area of the elastic block as it is proportional to the stiffness (k) of the spring. The Hookean oscillator should also demonstrate a higher quality factor and lower damping of the resonance in a vacuum.

We propose that the damping mechanism in graphene aerogels is based on the elastic scattering phenomena analogous to Thomson scattering[40], in which the amorphous porous structure works as a diffractive diffuser of mechanical waves. In this
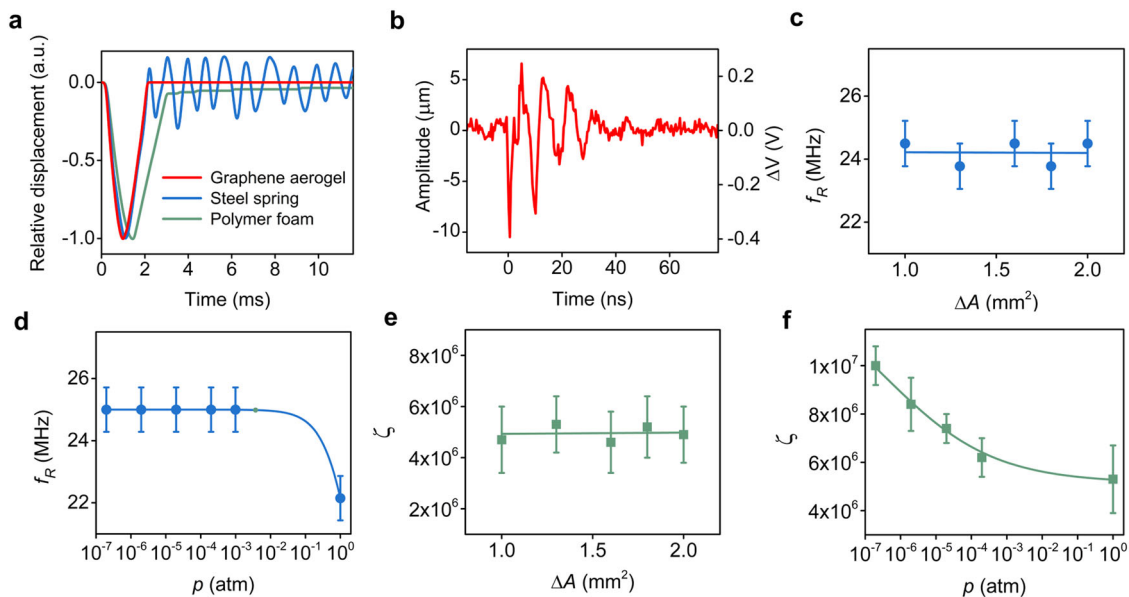
5

Fig. 4 Dynamic mechanical response of graphene aerogels. a Comparison of mechanical responses of elastic, plastic materials with graphene aerogel on the impact of a bouncing ball. **b** The natural resonance of a graphene aerogel block of the size of 2 mm × 1 mm × 2 mm on the mechanical impact. The amplitude was determined from the voltage response of the sample at a constant current of 100 mA. **c, d** Resonant frequency of graphene aerogel blocks as a function of the cross-section area at a constant sample thickness of 2 mm (**c**) and pressure (**d**). **e, f** Damping ratio dependence on the cross-section area (**e**) and pressure (**f**). Error bars represent the standard deviation in the measurements of ten different samples.

mechanism, the kinetic energy of the mechanical impact is elastically distributed into vibrations of individual pores of the aerogel. This process is very fast and frequency-independent. The mechanical waves are elastically diffusing in the material through the pore vibrations of interconnected cellular springs and the dynamic rippling of free-standing graphene walls[39,41], and consequently inelastically damped through a phonon and plasmon[42] damping on the longer time scales[43]. As the mechanical waves propagate in all directions, the longitudinal waves parallel to the direction of the impact decrease in the amplitude in the sample, resulting in fast damping of the whole sample vibrations. As long as the cross-section of the sample is significantly larger than the pore size, the scattering process is not affected by the change of the cross-section area of the sample. The elastic damping process is also expected to become more efficient and faster in a vacuum because the energy dissipation processes (e.g., residual gases and adsorbed molecules) that degrade the elasticity of the material are reduced.

Conclusion

In conclusion, we have shown that atomically thin graphene cellular materials demonstrate strikingly different elastic behavior than conventional bulk materials. The covalently cross-linked graphene aerogels demonstrate anomalous elastic mechanical properties, which allow them to be rapidly elastically compressed and stretched over an unprecedentedly broad range of strain and stress. The observed fast mechanical response and nanosecond damping in the graphene aerogels exhibit near-perfect elastic collisions and mechanical wave propagations in a macroscopic material. Our results provide new avenues for the construction of strong and flexible ultralight materials, superfast vibration dampers, sensors, and wearable electronic devices.

Methods

Synthesis of graphene aerogels. Graphene aerogels were prepared from graphene oxide via hydrothermal synthesis and freeze-drying. A mixture of commercially available graphene oxide (Graphenea, XFNANO) and deionized water in ratio 2:1 was sonicated for 30 min (Graphenea)/1 h (XFNANO) to get a

homogeneous dispersion. The mixture was transferred into a Teflon-lined stainless steel autoclave and annealed in an oven at 180 °C for 6 h. The hydrothermal process resulted in the reduction and self-assembly of graphene oxide sheets into a 3D hydrogel structure. The hydrogel was washed with DI water and freeze-dried at −70 °C in a vacuum (2×10^{-1} mBar) for 16 h to get a reduced graphene oxide aerogel. The as-prepared aerogel was annealed at 1300 °C in a vacuum furnace (1×10^{-4} mBar) to obtain the superelastic graphene aerogel (Supplementary Method 1). The temperature was monitored by a pyrometer (Optris, model CSlaser 2MH CF2).

Material characterization. Scanning electron microscopy of the graphene aerogels was carried out using a TESCAN MAIA3 SEM. In situ compression micrographs of the graphene aerogels were done using a nanomanipulator (Kleindiek MMA3A-EM).

Raman spectra were obtained using a Raman system (Renishaw inVia Reflex) with HeCd laser (λ = 442 nm). The elemental composition of graphene aerogels was done using X-ray photon spectroscopy (Kratos Analytical Ltd) with a detection limit of 0.6 atomic percent.

All electrical contacts between graphene aerogels and copper wires/tapes were done using a silver epoxy glue (MG chemicals 8331-14G). Electrical characterizations (electrical conductivity) were measured by a Keithley source measure unit (Model 236 and 237) using either a constant current (0.1–0.5 A) or constant voltage (0.01 V) mode.

Mechanical testing. A relative change in height and length (strain) of graphene aerogels was measured using an optical microscope. The compression testing up to 3 MPa was done using a homemade press (Supplementary Method 2). The high-pressure experiments were performed inside a diamond anvil cell, where the pressure was measured from the shift of the fluorescence of the ruby R 1 line. The tensile testing was done using a homemade hanging setup (Supplementary Fig. 4 and Supplementary Movies 1, 2). The edges of the sample were epoxy glued to metal rods. The force application was done by gravitational force exerted by a container with varying amounts of water (Supplementary Method 3). The stress-strain data shown in Figs. 2 and 3 are a summary of 20 samples measured in the uniaxial compression, three samples in the diamond anvil cell, and two samples in the uniaxial tension tests (Supplementary Table 4). Each of the measured points in the figures represents an average value of ten load-unload cycles except for the last two points at the breakpoint.

The optical measurements of a sample hit by a falling ball (mass 0.02 g, radius 1 mm) from 30 cm height were done using a high-speed camera (Photron Fastcam Mini UX100) equipped with a 40-mm objective at the resulting magnification of 0.7 and a framerate of 10,000 fps.

The change in voltage of a sample induced by the mechanical impact of a metal rod was measured using an oscilloscope (Tektronix TDS 620B) by applying a constant current of 0.1–0.3 A (Agilent E3631A) (Supplementary Method 5).

Data availability

The data that support the findings of this study are available from the corresponding author upon reasonable request.

References

1. Gao, H.-L. et al. Super-elastic and fatigue resistant carbon material with lamellar multi-arch microstructure. *Nat. Commun.* **7**, 12920 (2016).
2. Zhao, K. et al. Super-elasticity of three-dimensionally cross-linked graphene materials all the way to deep cryogenic temperatures. *Sci. Adv.* **5**, eaav2589 (2019).
3. Vatankhah-Varnosfaderani, M. et al. Mimicking biological stress–strain behaviour with synthetic elastomers. *Nature* **549**, 497–501 (2017).
4. Buehler, M. J. Materials by design—A perspective from atoms to structures. *MRS Bull.* **38**, 169–176 (2013).
5. Qiu, L. et al. Extremely low density and super-compressible graphene cellular materials. *Adv. Mater.* **29**, 1701553 (2017).
6. Walsh, J. B., Brace, W. F. & England, A. W. Effect of porosity on compressibility of glass. *J. Am. Ceram. Soc.* **48**, 605–608 (1965).
7. Darling, K. A. et al. Nanocrystalline material with anomalous modulus of resilience and springback effect. *Scr. Mater.* **141**, 36–40 (2017).
8. Groß, J. & Fricke, J. Scaling of elastic properties in highly porous nanostructured aerogels. *Nanostructured Mater.* **6**, 905–908 (1995).
9. Liu, D. et al. Towards understanding the influence of porosity on mechanical and fracture behaviour of quasi-brittle materials: experiments and modelling. *Int. J. Fract.* **205**, 57–72 (2017).
10. Zhang, W. et al. Preparation and properties of silicone rubber materials with foam/solid alternating multilayered structures. *Polym. J.* **53**, 619–631 (2021).
11. Wu, Y. et al. Three-dimensionally bonded spongy graphene material with super compressive elasticity and near-zero Poisson's ratio. *Nat. Commun.* **6**, 6141 (2015).
12. Worsley, M. A. et al. Synthesis of graphene aerogel with high electrical conductivity. *J. Am. Chem. Soc.* **132**, 14067–14069 (2010).
13. Xiao, J., Tan, Y., Song, Y. & Zheng, Q. A flyweight and superelastic graphene aerogel as a high-capacity adsorbent and highly sensitive pressure sensor. *J. Mater. Chem. A* **6**, 9074–9080 (2018).
14. Hu, K., Szkopek, T. & Cerruti, M. Tuning the aggregation of graphene oxide dispersions to synthesize elastic, low density graphene aerogels. *J. Mater. Chem. A* **5**, 23123–23130 (2017).
15. Jeong, Y. R. et al. Highly stretchable and sensitive strain sensors using fragmentized graphene foam. *Adv. Funct. Mater.* **25**, 4228–4236 (2015).
16. Pang, Y. et al. Flexible, highly sensitive, and wearable pressure and strain sensors with graphene porous network structure. *ACS Appl. Mater. Interfaces* **8**, 26458–26462 (2016).
17. Li, C., Ding, M., Zhang, B., Qiao, X. & Liu, C.-Y. Graphene aerogels that withstand extreme compressive stress and strain. *Nanoscale* **10**, 18291–18299 (2018).
18. Cheng, Y. et al. Enhanced mechanical, thermal, and electric properties of graphene aerogels via supercritical ethanol drying and high-temperature thermal reduction. *Sci. Rep.* **7**, 1439 (2017).
19. Kashani, H., Ito, Y., Han, J., Liu, P. & Chen, M. Extraordinary tensile strength and ductility of scalable nanoporous graphene. *Sci. Adv.* **5**, eaat6951 (2019).
20. Qiu, L., Liu, J. Z., Chang, S. L. Y., Wu, Y. & Li, D. Biomimetic superelastic graphene-based cellular monoliths. *Nat. Commun.* **3**, 1241 (2012).
21. Worsley, M. A. et al. Synthesis and characterization of highly crystalline graphene aerogels. *ACS Nano* **8**, 11013–11022 (2014).
22. Xu, Y., Sheng, K., Li, C. & Shi, G. Self-assembled graphene hydrogel via a one-step hydrothermal process. *ACS Nano* **4**, 4324–4330 (2010).
23. Farivar, F. et al. Unlocking thermogravimetric analysis (TGA) in the fight against "Fake graphene" materials. *Carbon* **179**, 505–513 (2021).
24. Schniepp, H. C. et al. Functionalized single graphene sheets derived from splitting graphite oxide. *J. Phys. Chem. B* **110**, 8535–8539 (2006).
25. Becerril, H. A. et al. Evaluation of solution-processed reduced graphene oxide films as transparent conductors. *ACS Nano* **2**, 463–470 (2008).
26. Chen, X. et al. Graphitization of graphene oxide films under pressure. *Carbon* **132**, 294–303 (2018).
27. Xiang, C. et al. Graphene nanoribbons as an advanced precursor for making carbon fiber. *ACS Nano* **7**, 1628–1637 (2013).
28. Gao, Z. et al. Graphene reinforced carbon fibers. *Sci. Adv.* **6**, eaaz4191 (2020).
29. Guo, F. et al. Highly stretchable carbon aerogels. *Nat. Commun.* **9**, 881 (2018).
30. Worsley, M. A. et al. Mechanically robust 3D graphene macroassembly with high surface area. *Chem. Commun.* **48**, 8428–8430 (2012).
31. Worsley, M. A. et al. High surface area, sp2-cross-linked three-dimensional graphene monoliths. *J. Phys. Chem. Lett.* **2**, 921–925 (2011).
32. Crisafulli, A., Khodayari, A., Mohammadnejad, S. & Fasano, M. Sliding dynamics of parallel graphene sheets: effect of geometry and Van Der Waals interactions on nano-spring behavior. *Crystals* **8**, 149 (2018).
33. Grandbois, M., Beyer, M., Rief, M., Clausen-Schaumann, H. & Gaub, H. E. How strong is a covalent bond? *Science* **283**, 1727–1730 (1999).
34. Cao, K. et al. Elastic straining of free-standing monolayer graphene. *Nat. Commun.* **11**, 284 (2020).
35. Ubbelohde, A. R. Hole and claw defects in graphite. *Nature* **180**, 380–380 (1957).
36. Zoldesi, C. I., Ivanovska, I. L., Quilliet, C., Wuite, G. J. L. & Imhof, A. Elastic properties of hollow colloidal particles. *Phys. Rev. E* **78**, 051401 (2008).
37. Frank, I. W., Tanenbaum, D. M., van der Zande, A. M. & McEuen, P. L. Mechanical properties of suspended graphene sheets. *J. Vac. Sci. Technol. B Microelectron. Nanometer Struct. Process. Meas. Phenom.* **25**, 2558–2561 (2007).
38. Lu, Q., Arroyo, M. & Huang, R. Elastic bending modulus of monolayer graphene. *J. Phys. Appl. Phys.* **42**, 102002 (2009).
39. He, Y. Z. et al. Dynamic ripples in single layer graphene. *Appl. Phys. Lett.* **98**, 063101 (2011).
40. Thomson, J. J. On electrical oscillations and the effects produced by the motion of an electrified sphere. *Proc. Lond. Math. Soc.* **s1-15**, 197–219 (1883).
41. Keşkekler, A. et al. Tuning nonlinear damping in graphene nanoresonators by parametric–direct internal resonance. *Nat. Commun.* **12**, 1099 (2021).
42. Buljan, H., Jablan, M. & Soljačić, M. Damping of plasmons in graphene. *Nat. Photonics* **7**, 346–348 (2013).
43. Yan, H. et al. Damping pathways of mid-infrared plasmons in graphene nanostructures. *Nat. Photonics* **7**, 394–399 (2013).
44. Lee, C., Wei, X., Kysar, J. W. & Hone, J. Measurement of the elastic properties and intrinsic strength of monolayer graphene. *Science* **321**, 385–388 (2008).
45. Banerjee, A. et al. Ultralarge elastic deformation of nanoscale diamond. *Science* **360**, 300–302 (2018).
46. Qian, D., Wagner, G. J., Liu, W. K., Yu, M.-F. & Ruoff, R. S. Mechanics of carbon nanotubes. *Appl. Mech. Rev.* **55**, 495–533 (2002).
47. Krawczynska, A. T., Chrominski, W., Ura-Binczyk, E., Kulczyk, M. & Lewandowska, M. Mechanical properties and corrosion resistance of ultrafine grained austenitic stainless steel processed by hydrostatic extrusion. *Mater. Des.* **136**, 34–44 (2017).
48. Okereke, M. I., Buckley, C. P. & Siviour, C. R. Compression of polypropylene across a wide range of strain rates. *Mech. Time-Depend. Mater.* **16**, 361–379 (2012).
49. Fan, J. & Chen, A. Studying a flexible polyurethane elastomer with improved impact-resistant performance. *Polymers* **11**, 467 (2019).
50. Papagelis, K. et al. In *GraphITA 2011* (eds. Ottaviano, L. & Morandi, V.) (Springer, 2012).
51. Nie, A. et al. Approaching diamond's theoretical elasticity and strength limits. *Nat. Commun.* **10**, 5533 (2019).
52. Moradi, M. & Aghazadeh Mohandesi, J. Mechanical behavior of carbon nanotube and graphene junction as a building block for 3D carbon nanostructures. *AIP Adv.* **5**, 117143 (2015).
53. Qu, S. et al. Tensile and compressive properties of AISI 304L stainless steel subjected to equal channel angular pressing. *Mater. Sci. Eng. A* **475**, 207–216 (2008).
54. Amjadi, M. & Fatemi, A. Tensile behavior of high-density polyethylene including the effects of processing technique, thickness, temperature, and strain rate. *Polymers* **12**, 1857 (2020).
55. Wang, Z. et al. Stretchable materials of high toughness and low hysteresis. *Proc. Natl. Acad. Sci. USA* **116**, 5967–5972 (2019).

Author contributions

M.S., P.K., and J.C. conceived and designed the experiments. M.S., P.K., and Z.A.Z. synthesized the graphene aerogels. M.S. and P.K. carried out the material characterization, mechanical and electrical measurements. M.M. and M.S. performed high-pressure experiments. M.C., M.P., and M.S. carried out the fast camera experiments. M.S., P.K., and J.C. analyzed the data and/or discussed the results. M.S. and J.C0 wrote the paper. All authors commented on the manuscript.

Competing interests

The authors declare no competing interests.

Additional information

Supplementary information The online version contains supplementary material available at https://doi.org/10.1038/s42005-022-00806-5.

Correspondence and requests for materials should be addressed to Jiří Červenka.

Peer review information *Communications Physics* thanks the anonymous reviewers for their contribution to the peer review of this work.

Reprints and permission information is available at http://www.nature.com/reprints

Publisher's note Springer Nature remains neutral with regard to jurisdictional claims in published maps and institutional affiliations.